Open Ceramics 14 (2023) 100351

Contents lists available at ScienceDirect

Open Ceramics

journal homepage: www.sciencedirect.com/journal/open-ceramics

Electrochemical performance of SiCN embedded carbon (SiCN–C) fiber mat electrodes for lithium-ion battery: Electrospinning polysilazane in air or protective atmosphere

Heloisa Ramlow [a,b,c], Cintia Marangoni [a], Günter Motz [b], Gurpreet Singh [c], Ricardo Antonio Francisco Machado [a,*]

[a] Graduate Program in Chemical Engineering, Federal University of Santa Catarina, Universitário Reitor João David Ferreira Lima Campus, 88040-900, Florianópolis, Santa Catarina, Brazil
[b] Department of Ceramic Materials Engineering, University of Bayreuth, Prof. R.-Bormann-Str. 1, 95447, Bayreuth, Bayern, Germany
[c] Department of Mechanical and Nuclear Engineering, Kansas State University, 66506, Manhattan, KS, USA

ARTICLE INFO

Handling Editor: Dr P Colombo

Keywords:
Ceramic anode
Electrode material
Polymer-derived ceramic

ABSTRACT

Here polysilazane/polyacrylonitrile fiber mats were manufactured by electrospinning in air or protective atmosphere. After pyrolysis, SiCN embedded carbon (SiCN–C) was tested as lithium-ion battery (LIB) electrode. Fibers electrospun in nitrogen are found to be thinner due to the slower solidification of the flying jet. XPS analysis confirmed that fibers electrospun in air incorporated a great oxygen content during shaping. The highest charge capacity of 773 mA h g^{-1} at 50 mA g^{-1} was recovered for SiCN–C electrospun in air. Oxygen increased the capacity due to its high character to attract Li^+ ions, but SiCN–C electrospun in air suffered voltage hysteresis. Contrariwise, the SiCN–C electrospun in nitrogen demonstrated stable cycling with a charge capacity of 299 mA h g^{-1} and 98% recovery of the initial capacity due to enhanced free carbon content. These findings make electrospinning very promising for the highly controlled production of freestanding SiCN fiber mat electrodes.

1. Introduction

Efficient utilization of future electronic devices will require increased storage capacities, long-term safety, and stability of rechargeable batteries. Among various rechargeable batteries technologies, the lithium-ion battery (LIB) continues to dominate mainly because of consistent specific energies of approximately 120 Wh kg^{-1}, low reduction potentials, and the small ionic size of a Li^+ ion (0.76 Å) which facilitates smooth intercalation and fast electrochemical kinetics [1].

Recent studies have investigated silicon-based covalent ceramics (such as SiCO or SiCN) prepared via the precursor-derived ceramic (PDC) process as potential electrode materials for LIB because of favorable electrochemical properties [2], such as reversible accommodation of Li^+ ions in a potential range of 0–2.5 V with high electrochemical capacities up to 900 mAh g^{-1} (despite that low capacities are also reported) and Coulombic efficiencies over 99% [3]. Particularly, PDCs with excess carbon such as C-rich SiCN have been shown to improve the electrochemical performance as LIB anode significantly due to sufficient nanocarbon clusters and free dangling bonds of silicon and carbon, which are active sites for the intercalating/de-intercalating of Li^+ ions, and the presence of nanoholes or nanochannels in the SiCN network, which improve electrochemical dynamic properties [4–9]. Although Dahn et al. filed a patent in 1996 for polysilazane-derived SiCN electrodes for LIBs [10], minimal research has compared the application of SiCO to these materials in LIBs.

Silicon-based PDCs are generally poor conductors of electronic/ionic current and the electrode preparation often requires the incorporation of conducting agents and binders on a metal current collector, thereby increasing the weight of the energy storage device [11]. However, future electrochemical energy storage devices must be lightweight to accommodate advances in wearable, flexible electronics [12]. Moreover, the addition of a conductive agent (considered a non-active phase for Li-ion storage) masks the real electrochemical performance of the electrode material [13]. Engineering electrode structures to enhance their ionic and electronic conductivity can significantly improve the electrochemical properties [14] and as a result, electrodes that are free of binder, conducting agents, and current collectors are desirable. For

* Corresponding author.
E-mail address: ricardo.machado@ufsc.br (R.A.F. Machado).

https://doi.org/10.1016/j.oceram.2023.100351
Received 12 October 2022; Received in revised form 6 March 2023; Accepted 23 March 2023
Available online 24 March 2023

example, freestanding fiber electrodes are advantageous due to their higher overall gravimetric energy density [15–17].

Non-woven fiber mats prepared via electrospinning and the PDC process have recently been considered electrode materials [18–22]. Electrospinning creates freestanding fiber mats that may be used as binder-free working electrodes. Since initial research published in 2007 [23,24], some progress has been made regarding PDC fiber mats shaped by electrospinning, but additional research is required, such as investigating the influence of the electrospinning atmosphere on PDC composition, especially for oxygen-sensitive polysilazanes typically electrospun in air [25–28]. Additional studies are required to understand the effect of nitrogen and oxygen and the structure-property relationship of SiCN on Li + ions' electrochemical storage to design effective polymer-derived SiCN fiber mat electrodes.

This work aims to investigate the electrochemical performance of SiCN fiber mats electrospun in air or protected nitrogen atmosphere and applied as LIB electrodes. Solutions containing polysilazane as the preceramic polymer and polyacrylonitrile (PAN) as the carbon source were shaped via electrospinning performed in air or protective atmosphere (nitrogen). After pyrolysis, SiCN with *in situ* synthesized free carbon was manufactured, and a single material was obtained resulting in SiCN embedded carbon fiber mats. To the best of our knowledge, this is the first known report that proposes SiCN electrospun fiber mats as electrodes for LIBs. The results of this work will provide a reference for designing the optimal composition of PDC-based fiber mat electrodes manufactured via the electrospinning process. Here we show that the atmosphere of the electrospinning process may influence the fiber mats regarding their morphology as demonstrated by electron microscopy, and composition as confirmed with XPS analysis. The fiber mats shaped in air showed a high electrochemical capacity as LIB electrodes due to the oxygen incorporation during electrospinning. Nevertheless, the fiber mats shaped in nitrogen showed excellent electrochemical stability and recovery of the initial reversible capacity after fast-cycling attributed to their high content of free carbon.

2. Material and methods

2.1. Electrospinning of precursor solutions and pyrolysis of fiber mats

The oligosilazane HTT1800 (Merck KGaA, Germany) was crosslinked via the reactions between N–H and Si–H groups available in the precursor using tetrabutylammonium fluoride 1 M in tetrahydrofuran (Sigma-Aldrich Co. LLC., Germany), calcium borohydride bis(tetrahydrofuran) (Sigma-Aldrich Co. LLC., Germany) and tetrahydrofuran 99.5% [29]. The selective crosslinking was used to obtain a solid polysilazane with increased molecular weight and improved electrospinnability as reported in a previous study by the authors based on a statistical optimization approach of polysilazane solution for electrospinning [30]. PAN 200 kDa (Polysciences, USA) was dried at 110 °C for 24 h before use. The electrospinning solution was prepared by first dissolving PAN in dimethylformamide 99.5% (Fischer Chemical, USA) at 100 °C for 3 h (PAN concentration in DMF of 6.54 wt% for SiCN–40C and 8.34 wt% for SiCN–70C samples), adding polysilazane and 3 wt% of dicumyl peroxide 98% (Sigma-Aldrich Co. LLC., Germany) considering the polysilazane concentration in DMF, followed by magnetic stirring for 12 h at room temperature, as shown in Fig. 1a. Table 1 presents the denominations of the samples investigated in this work.

The solution was placed in a syringe coupled with a 21 G metallic needle clamped to a high-voltage power supply that applied approximately 24 kV and was fixed approximately 23.5 cm from the collector. The sample was extruded at a flow rate of approximately 0.9 mL h^{-1} controlled by a pump. The polymer solutions were electrospun in two different devices: one device was in air with a relative humidity of approximately 60%, and the other device was inside a glove box with a protective atmosphere (i.e. nitrogen atmosphere), as shown in Fig. 1b. As-spun mats were prepared for pyrolysis as presented (Fig. 1c), placed in a tubular furnace, and heated up to 1200 °C for 1 h with a heating rate of 5 °C min^{-1} in a nitrogen atmosphere. Ceramic fiber mats were obtained as shown in Fig. 1d. For comparison, SiCN (electrospun in

Table 1
Denomination of the samples investigated in this work.

Sample name	Polymer concentration in solution for electrospinning (wt%) (PAN + polysilazane)	Polysilazane:PAN concentration (wt %)	Electrospinning atmosphere
SiCN–40C-a	17.5	60:40	Air
SiCN–40C-i	17.5	60:40	Protective (inert -nitrogen)
SiCN–70C-a	13	30:70	Air
SiCN–70C-i	13	30:70	Protective (inert -nitrogen)

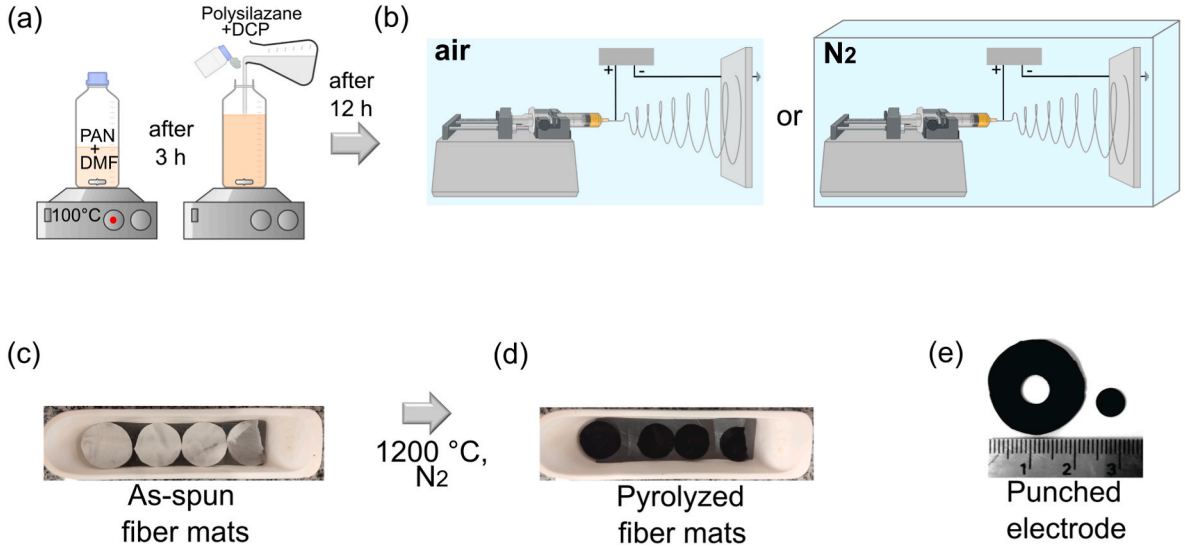

Fig. 1. Schematic diagram of the experimental process of this work including (a) precursor solution preparation, (b) electrospinning in air or protective atmosphere (nitrogen), (c) preparation of as-spun fiber mats for pyrolysis, (d) pyrolyzed fiber mats and (e) punching of fiber mat electrode.

protective atmosphere) and carbon (electrospun in air) fiber mats, prepared respectively from polysilazane and PAN, were also manufactured under similar conditions.

2.2. Characterizations

Scanning electron microscopy (SEM) was used to observe the morphology of the electrospun mats. Using EVO MA10 SEM (Zeiss, Germany) with an acceleration voltage of 5 kV, the fiber diameter was evaluated from four SEM images that randomly measured 100 fibers of each sample using open-source ImageJ software. X-ray photoelectron spectroscopy (XPS) was performed to analyze the composition of the electrospun mats. The XPS spectra were obtained with a Thermo Scientific Al $K\alpha^+$ ion beam with an energy of 1486.6 eV and a spot size of 400 μm (Chanhassen, USA). Surface contamination of the ceramic fiber mats was removed via surface sputtering with argon at 3.0 keV for 2 min. The Si–C–N–O + C_{free} composition was based on the empirical formula normalized on silicon considering 1) four chemical bonds of Si, 2) all oxygen and nitrogen linked to Si, 3) remaining Si linked to C, and 4) remaining carbon is free.

2.3. Electrode preparation and electrochemical energy storage measurement

The electrospun mats were used as freestanding electrodes in LIB half-cells, in which a lithium metal electrode (14.3 mm diameter and 75 μm thick) was utilized as both the counter and reference electrode. This configuration provides a stable reference potential with a large specific capacity, affording a very large reservoir of capacity so that the reactions at the working electrode are not limited by the capacity available at the counter electrode [31]. As shown in Fig. 1e, a disk electrode with an approximate diameter of 6.35 mm was punched out from the pyrolyzed mat and used as the working electrode. The electrolyte solution was a mixture of 1 M lithium hexafluorophosphate ($LiPF_6$) in 1:1 dimethyl carbonate:ethylene carbonate vol% (Sigma Aldrich, USA). A glass fiber separator (19 mm diameter, 25 μm thick) separated the two electrodes as they were pre-soaked with the electrolyte. The batteries were assembled in LIR-2032 coin cells in a glove box filled with argon 99.9% and tested using a multichannel BT 2000 Arbin test unit (College Station, USA) between 10 mV and 2.5 V vs. Li/Li^+. The cells were subjected to symmetric cycling at current densities of 50, 100, 200, 400, 600, and 800 mA g^{-1} for 10 cycles each followed by a current density of 50 mA g^{-1} for 40 cycles. The capacity was represented in mAh g^{-1} considering the anode mass, and the Coulombic efficiency (%) was calculated as the ratio of discharge capacity after full charge and charge capacity of the same cycle.

3. Results and discussion

SEM images of the pyrolyzed samples showed the morphology of the resulting SiCN fiber mats after electrospinning and polymer to ceramic transformation. Fig. 2 shows that the fiber diameter was 937 ± 235 nm for SiCN–40C-a, 153 ± 20 nm for SiCN–40C-i, 833 ± 237 nm for SiCN–70C-a, and 150 ± 26 nm for SiCN–70C-i. The fibers electrospun in nitrogen atmosphere had a much thinner diameter (approx. 83%) when compared to the fibers electrospun in air, attributed to the influence of 60% relative humidity in the air. Despite that electrospinning is a very fast process, research has shown that the influence of moisture in the air is not limited [32]. The presence of water molecules in the air discharges the electrospinning jet due to molecular polarization; the jet is less vigorously subjected to whipping instabilities and less elongated. For a system composed of hydrophobic PAN, the high humidity in the air led to early solidification resulting in thicker diameters and the suppression of bead-on-string morphologies. The fibers electrospun in a protective atmosphere were uniform and smoother than fibers obtained by electrospinning performed in air, as also reported in a previous study that investigated the electrospinning of organic fibers [33]. However, the presence of solvent molecules inside the electrospinning chamber delayed the solidification of the fibers due to some solvent absorption into the jet and polymer plasticizing, and, consequently, favoring the apparition of bead-on-string fibers. The histogram of the fiber diameter was better normally distributed compared to the histogram of fiber diameter electrospun in the air, which showed some fiber diameter difference. This was not observed with polysilazane-derived SiCN fibers, which showed a homogeneous morphology when electrospun in nitrogen atmosphere attributed to the high polymer concentration hindering further jet elongation (Fig. S1a). In contrast, carbon fibers electrospun in air also showed some irregularities due to the high moisture content in

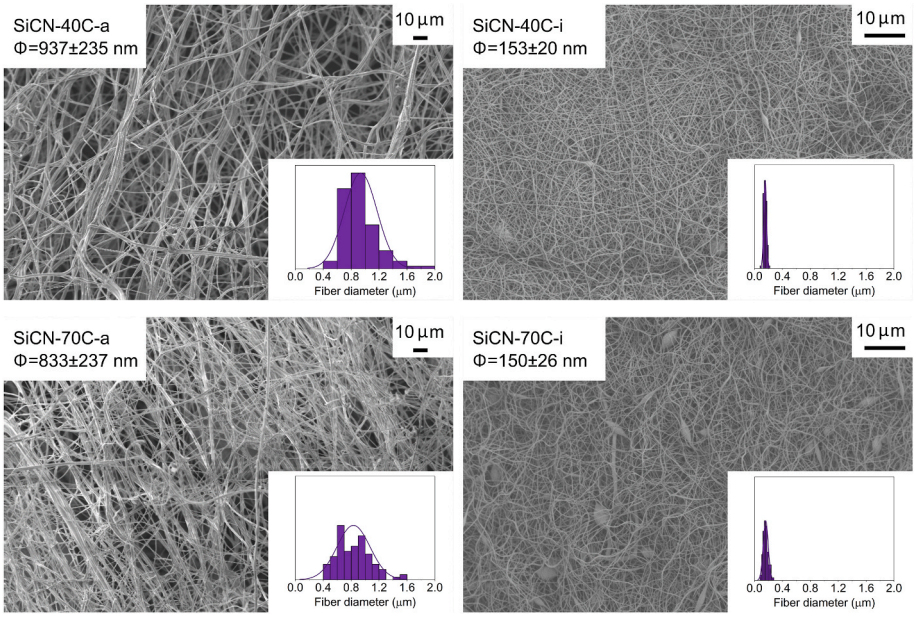

Fig. 2. SEM images, respective fiber diameter (Φ) and histogram of pyrolyzed fiber mats electrospun in air (SiCN–40C-a and SiCN–70C-a) or protective atmosphere (SiCN–40C-i and SiCN–70C-i). Fibers electrospun in protective atmosphere are smoother, more uniform, and thinner than samples realized by conventional electrospinning performed in air.

the air during electrospinning (Fig. S1b).

Later, the as-prepared polymer-derived SiCN fiber mats were used as the working electrodes in LIBs coin cell in a half-cell configuration. The porous structure and microstructure provided by the electrospinning and PDC approach allowed the liquid electrolyte to fully penetrate the electrode thereby providing a shorter path for solvated ions to be transported onto the surface of the fibers [11]. Fig. 3 shows the voltage plots of the first and second cycles at a current density of 50 mA g^{-1}. Ideally, the discharge/charge curves should be identical in opposite directions, but the voltage profiles showed that the first cycle had experienced irreversible capacity decay primarily for the mats electrospun in air since the increased voltage was needed for the discharge of the same capacity. Irreversibility in these materials typically occurs because of the formation of poorly reversible structures of solvated lithium (e.g. Li_2O_3 due to the presence of oxygen) and solid electrolyte interphase (SEI) formation related to the surface area [34–36].

Different charge-discharge profiles were observed for fiber mat electrodes depending on the electrospinning atmosphere in which they were processed. For example, a pronounced voltage hysteresis was detected for SiCN–40C-a and SiCN–70C-a samples, with a higher voltage being required for Li^+ extraction than for Li^+ insertion due to electrochemical polarization arising from the internal resistance of the electrode materials [37]. Despite the low current, pronounced voltage hysteresis of up to 2.5 V was observed for the electrospinning conducted in air, which results in low energy efficiency. However, for the electrospinning conducted in a protective atmosphere, the voltage hysteresis of SiCN–40C-i and SiCN–70C-i was suppressed and the major part of the charge was recovered at a potential below 1 V. This was most likely due to the existence of different potential states for Li-ion insertion [35,38]. For SiCO electrodes, which have structures similar to SiCN, voltage hysteresis was attributed to a difference in the electrochemical potential of the Li^+ ions at the SiCO-electrolyte interface, and the electrochemical potential of the Li^+ ions within the electrolyte that was in equilibrium with the lithium metal counter electrode [39]. The voltage profile of the SiCN electrode also exhibited some voltage hysteresis (Fig. S2a) as contrasted with the carbon electrode (Fig. S2b), which did not show significant hysteresis due to its structural uniformity during Li-ion charging and discharging [38,40]. The fiber mats electrospun in air showed a higher capacity compared to fiber mats electrospun in a protective atmosphere due to the higher content of oxygen as explained hereafter.

Despite that XPS is a surface analysis, the fibers prepared here are ultrathin materials and, therefore this technique can be considered as appropriate for the identification and quantification of the elements present in the fiber as has been conducted in other studies on ultrathin PDC fibers [41,42]. The XPS survey scan (Fig. S3), confirmed the presence of silicon, carbon, nitrogen, and oxygen in SiCN fiber mat materials. XPS spectra of the electrospun fiber mats also clearly showed distinct Si 2p, C 1s, N 1s, and O 1s peaks according to the electrospinning atmosphere. The XPS elemental composition for various specimens is summarized in Table S1. High-resolution XPS spectra, plotted in Fig. 4, show the bonding of the pyrolyzed fiber mats after the curve fitting of peaks. Spectra under the Si 2p band indicated the presence of Si–N (101.9 eV), Si–C (102.7 eV), and Si–O (103.5 eV) peaks [11,43]. In addition, C–Si (284.0 eV), C–C (284.9 eV), and C═O (286.0 eV) peaks were observed in the C 1s band and N–Si (398.1 eV) in the N 1s band [38]. The increased amount of carbon in the fiber mats electrospun in the protective atmosphere leads to higher intensity of the C–C peak, suggesting an increased possibility of a free carbon phase. Indeed, PAN-derived carbon fibers showed mostly the presence of sp^2-carbon (84.13 at%) (Fig. S4). The O 1s band was fitted with two peaks at 532.4 eV and 534.0 eV corresponding to O–Si and C═O, respectively [3]. The fiber mats electrospun in air showed a significant increase in oxygen content (i.e., 45.61 at% and 12.60 at% for SiCN–40C-a and SiCN–40C-i, respectively; 31.14 at% and 19.91 at% for SiCN–70C-a and SiCN–70C-i, respectively). Oxygen replaced nitrogen in the SiCN structure, particularly nitrogen present on the fiber surface after electrospinning in air since the surface atoms are more easily detected by XPS analysis. However, it is here highlighted that the fiber core when electrospun in air can be different from the fiber surface and oxygen was probably

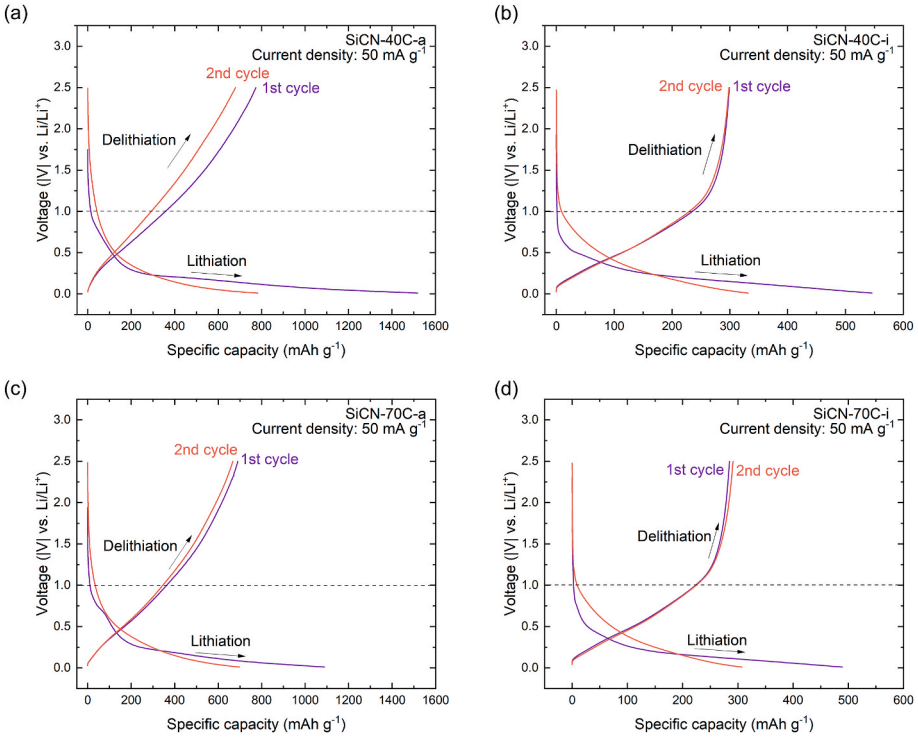

Fig. 3. Voltage profiles with 1st and 2nd charge-discharge cycles of the (a–d) SiCN–40C-a, SiCN–40C-i, SiCN–70C-a, and SiCN–70C-i fiber mat electrodes. Despite the enhanced capacity, SiCN–C electrodes electrospun in air suffered higher voltage hysteresis compared to SiCN–C electrodes electrospun in protective atmosphere.

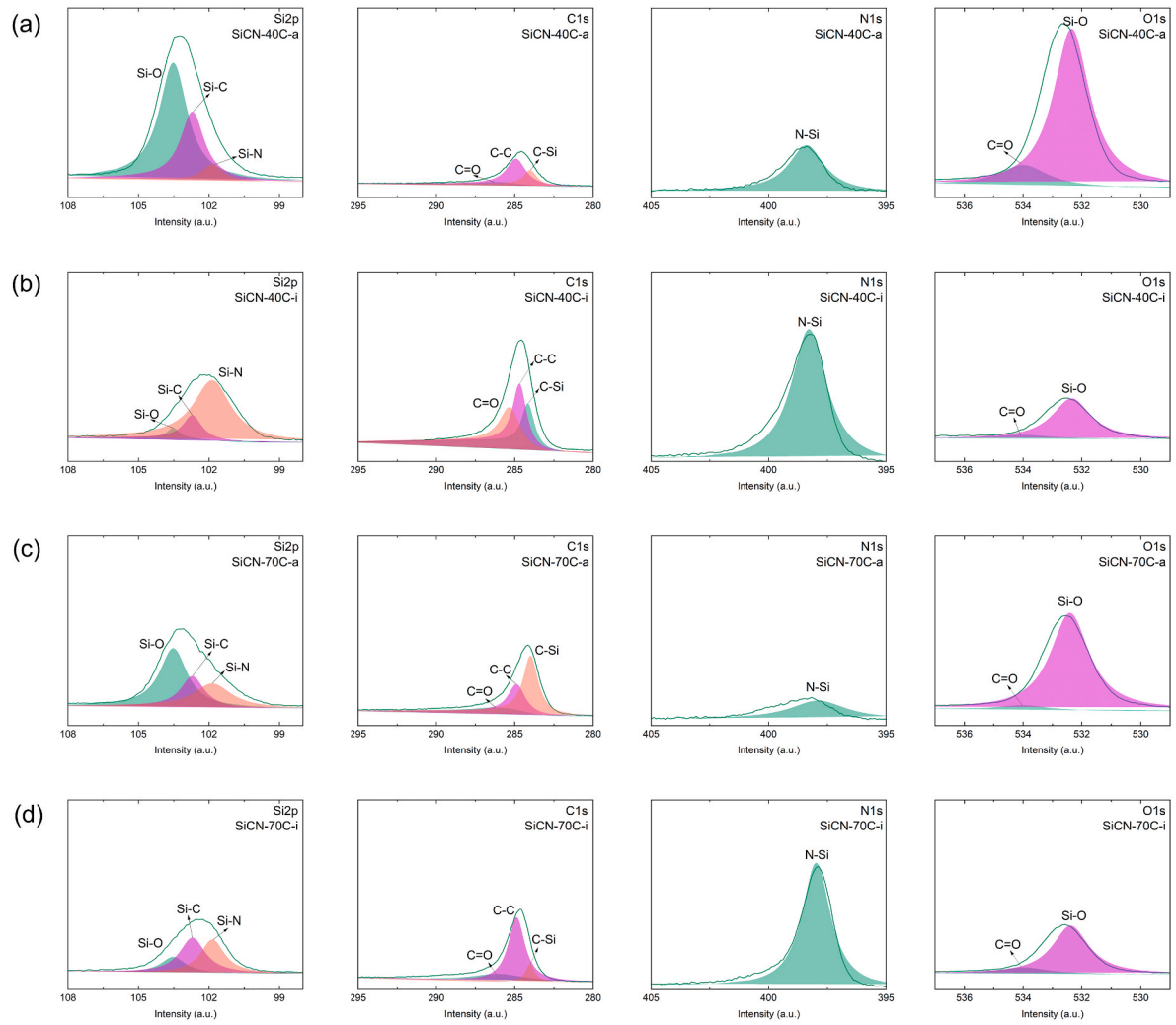

Fig. 4. High-resolution XPS spectra of the (a) SiCN–40C-a, (b) SiCN–40C-i, (c) SiCN–70C-a, and (d) SiCN–70C-i fiber mats. Electrodes electrospun in air incorporated a great oxygen content during shaping compared to electrodes electrospun in protective atmosphere.

concentrated only on the fiber surface. The increased amount of oxygen in samples electrospun in air (more than 30 at%), correlated to a decreased amount of carbon probably because of partial combustion of carbon. Additionally, the irreversible capacity and voltage hysteresis observed in the voltage profiles of the SiCN–C electrodes electrospun in air (Fig. 3) may be due to the high oxygen content present in these samples [39].

For SiCN–40C-a, SiCN–40C-i, SiCN–70C-a, and SiCN–70C-i fiber mats, an initial charge of 773 mAh g^{-1}, 299 mAh g^{-1}, 690 mAh g^{-1}, and 285 mAh g^{-1} was obtained with Coulombic efficiency of 51%, 55%, 63%, and 58%, respectively (Table S2). The electronegativity values of oxygen and nitrogen are 3.5 and 3.0, respectively. The SiCN–40C-a and SiCN–70C-a electrodes showed increased levels of oxygen coming from the air during electrospinning since silicon more readily reacts with electronegative oxygen than nitrogen. High lithiation capacities observed here for SiCN–40C-a and SiCN–70C-a are due to the increased attraction of Li^+ by oxygen in the Si–C–O network because of the pronounced ionic character of Si–O bonds with high electron density on the oxygen atom. A previous study has shown that when oxygen is replaced by nitrogen (e.g., high N/O ratio in SiCNO), the ceramic becomes less attractive for Li^+ ions due to the more covalent character of Si–N bonds and lower electron density on the nitrogen atom resulting in less capture of Li^+ in the ceramic matrix [44], as confirmed by the decreased electrochemical performance of the LIB electrodes in the current study. Similarly, the high capacity of C-rich SiCN prepared in air has been previously attributed to the presence of high content of disordered carbon and the presence of oxygen in the SiCN phase [6]. Here, when oxygen was introduced to the SiCN system and the O/N ratio was 14.2 and 12.6 respectively for SiCN–40C-a and SiCN–70C-a, respectively, the reversible capacity of the anodes was increased and higher initial capacities higher than 600 mA h g^{-1} were obtained [45]. The O/N ratio of SiCN–40C-i and SiCN–70C-i was respectively 1.5 and 2.1.

Previous research focused more on SiCO fiber mat electrodes than SiCN systems for LIBs. For example, polysiloxane-derived SiCO electrodes shaped by electrospinning have shown a first-cycle charge capacity ranging from 400 to 924 mA h g^{-1} [3,18,21,22,46]. In another work, a SiCN/graphite ceramic composite was fabricated by pyrolyzing a mixture of commercial-grade graphite powder (75 wt%) with a crosslinked polysilazane (25 wt%). This material had a charge capacity of 266 mA h g^{-1} and Coulombic efficiency of 62% [35], which is very similar to the SiCN–70C-i electrode prepared in this work (285 mAh g^{-1} and 58%).

In terms of Li^+ insertion/extraction, the materials exhibited higher capacity than that of the sum of components SiCN and carbon. Free carbon domains in the SiCN–C materials, derived from PAN and some amount from polysilazane, are supposed to be active sites for Li^+ insertion [47], while the amorphous structure of SiCN provides a pathway for Li^+ transfer, resulting in a synergistic effect of the SiCN–C electrodes. It is supposed that Li^+ insertion was firstly absorbed in the nanovoid sites, and then it was accommodated by the Si–C–N

tetrahedral units, free carbon, and topological defects at the edge of or within the segregated carbon network [48]. Moreover, as already mentioned, the nano-holes or nano-channels in the SiCN network provide many smooth Li^+ transfer channels, which improved the electrochemical dynamic properties.

For SiCN–C samples, the free carbon phase played likely a dominant role in bringing 1st cycle irreversible capacities due to Li^+ capturing in some pores and voids between carbon layers [44]. The relationship between the charge capacity and the carbon content was observed by diminishing 1st cycle irreversible capacity with higher carbon precursor content (Table S2). Carbon electrodes such as graphite have a low theoretical capacity of 372 mAh g^{-1} [49], as also observed for the carbon electrode prepared here with a charge capacity of 176 mAh g^{-1} in the 1st cycle. Thus, a certain equilibrium between the ceramic and carbon has to be maintained to achieve high capacity and stable performance concerning continuous Li^+ insertion/extraction. The SiCN anode showed very low charge capacities (6 mAh g^{-1}) with Coulombic efficiency lower than 80% due to its low electrical conductivity resulting from low free carbon content (C–C) (Fig. S4), which is following the literature [50,51]. The electrochemical capacity in SiCN was due to reversible Li^+ adsorption in the small amount of disordered carbon phase, a phenomenon called intercalation. Another phenomenon is the conventional alloying reaction of Li^+ with Si, which involves the breakage/distortion of Si–Si bonds to generate new Si–Li bonds. The alloying occurring in Si-based anodes may result in material delamination, particle cracking, recurrent dynamic creation of SEI layers, and ineffective electron transfer [52], however, these drawbacks were not observed with the SiCN–C anodes prepared here. The charge capacity in 1st cycle of SiCN electrodes is usually based on electrodes prepared by the screen-printing method with values of 313 mA h g^{-1} for 3D-CNT SiCN [51], 447 mA h g^{-1} for C-rich SiCN [8], and 900 mA h g^{-1} for NaOH-treated SiCN [53]. These values are higher than observed in the present work, however, the elimination of conducting agents, collector, binder, and solvents obtained with freestanding mats could provide positive environmental impacts and cost reduction.

In the second cycle, the electrodes showed a Coulombic efficiency of 87% (SiCN–40C-a), 90% (SiCN–40C-i), 96% (SiCN–70C-a), and 95% (SiCN–70C-i). The lower Coulombic efficiency observed for SiCN–40C-a was attributed to lithium reacting with oxygen present in their structure generating Li_2O_3, as mentioned previously, and also to lower free carbon content. For SiCN–70C-a and SiCN–70C-i, the efficiency was very similar due to the high carbon content present in these samples.

Differential capacity plots (Fig. 5), showed Li^+ ions diffusing in or out of the SiCN–C electrodes at a given voltage with distinct regions: a sharp cathodic peak around 0.02–0.15 V, corresponding to Li^+ insertion into disordered carbon [5,11,50,54]; a sharp cathodic peak at 0.2 V, reflecting $SiOC/SiO_x$ lithiation since this was observed for SiCN–40C-a and SiCN–70C-a containing high oxygen content [55,56]; and a broad cathodic peak at 0.7–0.8 V, indicating the availability of multiple Li-ion intercalation phases in the ceramic materials and SEI formation [57]. The broad anodic region at 0.07–0.95 V was ascribed to the interaction between Li^+ and the Si–N and Si–O network [58]. Moreover, the materials electrospun in nitrogen, (i.e., SiCN–40C-i and SiCN–70C-i), demonstrated a broad cathodic peak at 0.42–0.5 V due to the lithiation and delithiation of Li^+ in the amorphous SiCN structure (Fig. 5b and d), since it was also observed in the SiCN electrode (Fig. S5a). Various peaks ranging from 0.67 to 1.07 V were also observed in the carbon fiber mat (Fig. S5b), due to the decomposition of the electrolyte and SEI formation [59,60]. The oxidation peak at 0.1 V observed in the carbon electrode, not observed in the SiCN–C electrodes, corresponds to Li^+ deintercalation from graphitic carbon [61]. In the second cycle, no peak was found in the profile of the SiCN–C electrodes, suggesting that no new phases were formed toward lithium intercalation and that a stable SEI was formed.

This study also tested the long-term stability and rate capability of the SiCN–C fiber mats were tested as electrode materials for LIBs. Fig. 6 shows the charge capacities of the samples at different current densities. When tested for cycling stability after 10 cycles at 50 mA g^{-1}, the SiCN–40C-a electrode showed decreased performance, and the charge capacity dropped to 521 mA h g^{-1} with Coulombic efficiency of 98%

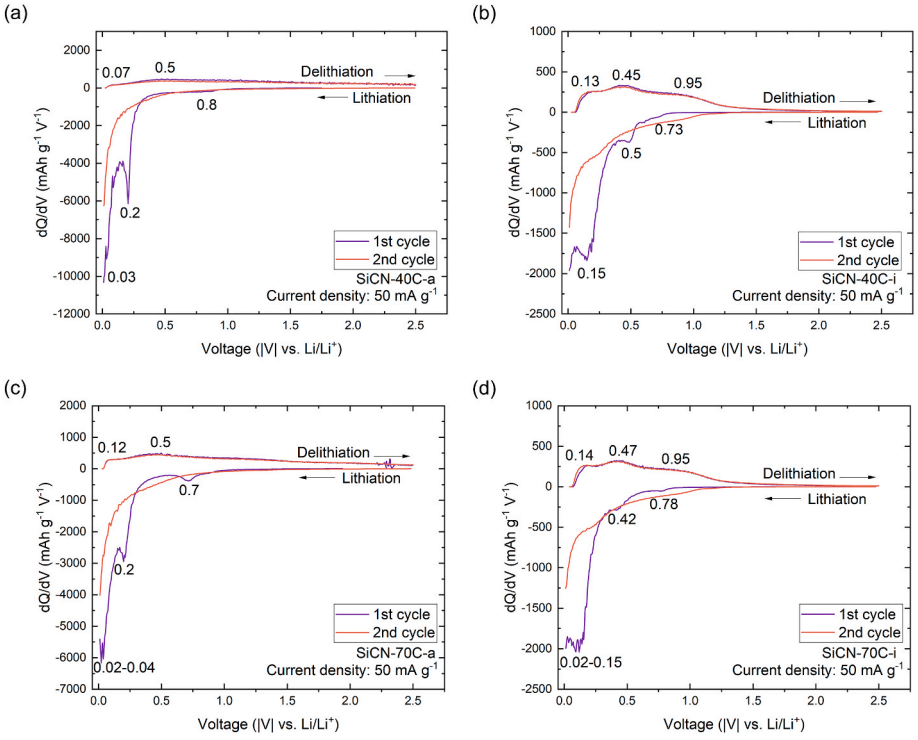

Fig. 5. Differential capacity (Q) and V (voltage) curves of the (a–d) SiCN–40C-a, SiCN–40C-i, SiCN–70C-a, and SiCN–70C-i electrodes. Each cathodic or anodic peak represents the characteristic region of reaction between Li-ion and the material.

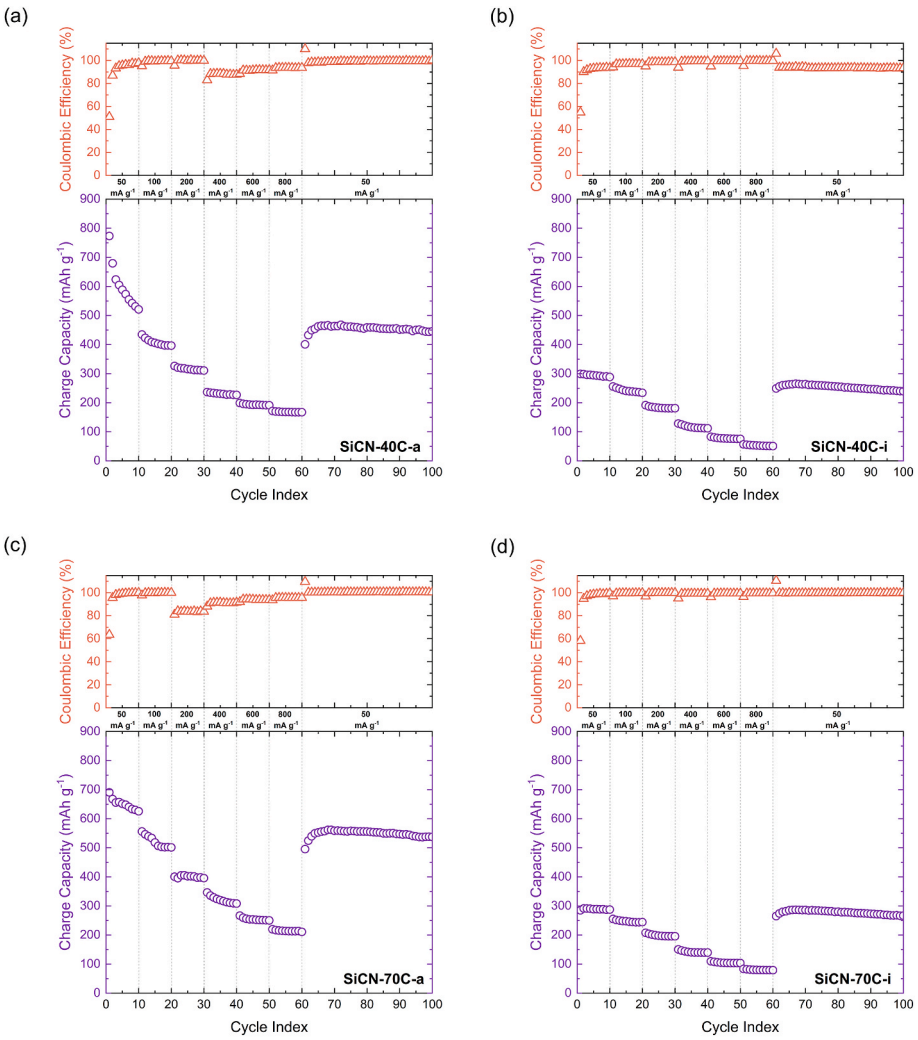

Fig. 6. Long-term stability and rate capability data of the SiCN–C for 100 cycles at different current densities. The cells were subjected to symmetric cycling at current densities of 50, 100, 200, 400, 600, and 800 mA g^{-1} for 10 cycles each followed by a current density of 50 mA g^{-1} for 40 cycles. The fiber mat electrodes showed a good capacity recovery feature with most of their original capacity regained when the current density decreased back to 50 mA g^{-1}.

compared to the SiCN–70C-a electrode with 629 mA h g^{-1} and Coulombic efficiency of 100%. In contrast, the samples electrospun in nitrogen showed similar capacities (i.e., 289 mA h g^{-1} and Coulombic efficiency of 94% for SiCN–40C-i; 288 mA h g^{-1} and Coulombic efficiency of 100% for SiCN–70C-a). These results demonstrate the influence of the Si–O network on the cycling stability of the PDC electrodes. Compared to fiber mats electrospun in protective atmosphere, the SiCN–40C-a and SiCN–70C-a electrodes showed a high capacity loss in the initial cycles due to excessive oxygen, which was considered a source of high irreversible capacity and significant voltage hysteresis [34]. Furthermore, the Coulombic efficiency of SiCN–70C-i was greater than SiCN–40C-a due to the increased free carbon content.

Increasing the current rate decreased the capacity of the SiCN–C electrodes, although most of their original capacity could be regained when the current density decreased back to 50 mA g^{-1}, proving that the materials have sufficient capacity recovery capabilities. Once the electrodes returned to lower current cycling, SiCN–40C-a, SiCN–40C-i, SiCN–70C-a, and SiCN–70C-i exhibited respectively 85%, 90%, 86%, and 98% of the initial capacity. Recovery of the initial reversible capacity after fast cycling showed that the materials were not damaged under the conditions of fast charge/discharge rates.

The SiCN electrode showed a capacity increase during the initial 10 cycles due to a structural reorganization (i.e., microstructure opening of the material during lithium intercalation/extraction to form new conducting paths) (Fig. S6a). However, the Coulombic efficiency decreased to 46% after seven cycles, meaning that more lithium ions were trapped, but not discharged by the SiCN matrix. After 10 cycles, the capacity of the SiCN electrode remained steady with no capacity decay because the active materials became stable and electrochemically reversible. There are two models proposed in the literature to explain the lithium storage mechanism in polymer-derived SiCO ceramics: mixed Si–C–O tetrahedra as active sites for Li^+ storage [62]; and interstitial spaces or edges between the graphene layers as the primary storing sites, the Si–O–C phase and the micropores [63]. Since the SiCN has a similar structure to the SiCO, the reversible capacity measured during the first discharge has been ascribed to the low content of free carbon (C–C) as presented in the XPS spectrum. Additionally, the carbon electrode exhibited steady capacity, but with low charge capacities at various current densities (Fig. S6b), which is following the literature on carbon-based anodes [52].

Of all the samples in this study, the SiCN–70C-a anode exhibited the best performance, delivering the highest capacity of about 518, 402, 320, 254, and 214 mA h g^{-1} at each of the applied current densities of 100, 200, 400, 600, and 800 mA g^{-1}, respectively. Carbon and oxygen contents in the SiCN–70C-a fiber mat provided additional Li-ion storage sites and improved the electrochemical properties of SiCN as already explained before. After 100 cycles, the SiCN–70C-a fiber mat electrode recovered most of the capacity with 538 mA h g^{-1} at 50 mA g^{-1}. This

value is comparable to or even higher than SiCO fiber mat electrodes (e.g., 281 mA h g^{-1} after 100 cycles at 35 mA g^{-1} [15], 500 mA h g^{-1} after 10 cycles at 50 mA g^{-1} [22], 543 mA h g^{-1} after 200 cycles at 50 mA g^{-1} [18], and 669 mA h g^{-1} after 80 cycles at 50 mA g^{-1} [46]). Compared to SiCN electrodes prepared by the screen printing method, the SiCN–70C-a electrode showed higher charge capacity, (e.g., 326 mA h g^{-1} at 100 mA g^{-1} after 30 cycles for 3D-CNT SiCN [51], 458 mA h g^{-1} at 20 mA g^{-1} after 134 cycles for C-rich SiCN [9], and 534 mA h g^{-1} at 72 mA g^{-1} after 100 cycles for C-rich SiCN [8]). Despite the irreversible capacity and voltage hysteresis, the SiCN–70C-a demonstrated attractive values of recovered capacity and outstanding cyclability for 100 cycles even at high current rates, making this material a promising anode material for energy devices.

In summary, we have demonstrated the manufacturing of SiCN–C freestanding fiber mats as stable and durable battery electrodes. The synergistic effect of the SiCN–C electrodes enhanced the electrochemical performance of LIBs, and the SiCN provided a pathway for Li^+ transfer, while free carbon improved electronic conductivity and the availability of active sites for Li^+. Nevertheless, a certain equilibrium between SiCN and carbon must be maintained to achieve high capacity and stable performance for continuous Li^+ insertion/extraction. In addition, the electrospinning atmosphere influenced the composition of the fiber mats. Electrospinning in air increase oxygen content in the polysilazane-derived SiCN, generating thus SiCNO ceramics. The SiCN–C-a fiber mat electrodes exhibited higher capacities at different current densities due to oxygen attracting the Li-ions to the materials. However, a correlation was observed between both the irreversible capacity and voltage hysteresis with the oxygen content of the SiCN–C electrodes shaped in air. The SiCN–C-i electrodes electrospun in protective atmosphere demonstrated improved cycling stability and significantly lower losses with increasing cycling current rates, which may be attributed to the presence of free carbon. These findings support electrospinning for the highly controlled production of SiCN fiber mat electrodes and even for other advanced applications and will prompt further research on PDC fibers.

4. Conclusions

This study explored the influence of the electrospinning atmosphere conducted in air or a protective atmosphere on SiCN fiber mats applied as LIB electrodes. Electron microscopy characterization revealed the morphology of smoother, more uniform, and thinner fibers when polysilazane was electrospun in nitrogen. In addition, various compositions in the SiCN–C fiber mats were obtained, as confirmed by XPS analysis. The SiCN–C materials showed promising electrochemical results for capacity and stability when compared to SiCN and carbon electrodes processed under similar conditions. The main reasons may be as follows: first, the improvement of capacity was due to the increasing free carbon content in the SiCN materials which are Li^+ ion active sites, and SiCN with smooth transfer channels for Li^+ mobility to attain a high charge current improving the electrochemical dynamic properties. Second, the SiCN fiber mats electrospun in air contained more oxygen that was easy to link with Li^+ ions, leading to the high capacity. Third, the improvement of cycle stability was due to the stable mechanical structure of SiCN–C fiber mats without breaking/disintegrating.

The strong dependence of the polymer-derived SiCN materials on their compositions and structures suggests the potential to enhance the electrochemical performance of these materials by molecular design and/or the control of material structure including the electrospinning atmosphere, as demonstrated in this work. The atmosphere in which the polymers are electrospun had a great influence on the morphology and composition of the ceramic fibers. The electrospinning and PDC processes could beneficially impact the preparation of Si-based fiber mat electrodes by controlling carbon, nitrogen, and oxygen content for electrochemical energy storage devices. Therefore, PDCs with enhanced Li-ion storage capacity, long-term safety, and stability may be developed as freestanding and binder-free fiber mats to meet the requirements of LIB electrodes.

Declaration of competing interest

The authors declare that they have no competing interests.

Acknowledgments

The authors thank CAPES and Deutscher Akademischer Austauschdienst (DAAD) for supporting this work within the project PROBRAL (nº 88887.368756/2019–00). This study was financed in part by the Coordenação de Aperfeiçoamento de Pessoal de Nível Superior - Brasil (CAPES) - Finance Code 001 and CNPq - Brasil (n° 442149/2018-2). GS thanks for financial support from National Science Foundation (NSF) Partnerships for International Research and Education (PIRE) grant number 1743701. HR thanks Sonjoy Dey for his help with cell assembly. The XPS analysis was performed in part in the Nebraska Nanoscale Facility: National Nanotechnology Coordinated Infrastructure and the Nebraska Center for Materials and Nanoscience (and/or NERCF), which are supported by the National Science Foundation under Award ECCS: 2025298, and the Nebraska Research Initiative.

Appendix A. Supplementary data

Supplementary data to this article can be found online at https://doi.org/10.1016/j.oceram.2023.100351.

References

[1] S. Mukherjee, S. Bin Mujib, D. Soares, G. Singh, Electrode materials for high-performance sodium-ion batteries, Materials 12 (2019) 1952, https://doi.org/10.3390/ma12121952.
[2] Q. Wen, Z. Yu, R. Riedel, The fate and role of in situ formed carbon in polymer-derived ceramics, Prog. Mater. Sci. 109 (2020), 100623, https://doi.org/10.1016/j.pmatsci.2019.100623.
[3] S. Bin Mujib, F. Ribot, C. Gervais, G. Singh, Self-supporting carbon-rich SiOC ceramic electrodes for lithium-ion batteries and aqueous supercapacitors, RSC Adv. 11 (2021) 35440–35454, https://doi.org/10.1039/d1ra05968h.
[4] Y. Feng, G.-X. Du, X.-J. Zhao, E.-C. Yang, Preparation and electrochemical performance of SiCN–CNTs composite anode material for lithium ion batteries, J. Appl. Electrochem. 41 (2011) 999–1002, https://doi.org/10.1007/s10800-011-0322-z.
[5] J. Kaspar, G. Mera, A.P. Nowak, M. Graczyk-Zajac, R. Riedel, Electrochemical study of lithium insertion into carbon-rich polymer-derived silicon carbonitride ceramics, Electrochim. Acta 56 (2010) 174–182, https://doi.org/10.1016/j.electacta.2010.08.103.
[6] M. Graczyk-Zajac, G. Mera, J. Kaspar, R. Riedel, Electrochemical studies of carbon-rich polymer-derived SiCN ceramics as anode materials for lithium-ion batteries, J. Eur. Ceram. Soc. 30 (2010) 3235–3243, https://doi.org/10.1016/j.jeurceramsoc.2010.07.010.
[7] L.M. Reinold, M. Graczyk-Zajac, Y. Gao, G. Mera, R. Riedel, Carbon-rich SiCN ceramics as high capacity/high stability anode material for lithium-ion batteries, J. Power Sources 236 (2013) 224–229, https://doi.org/10.1016/j.jpowsour.2013.02.046.
[8] M. Storch, D. Vrankovic, M. Graczyk-Zajac, R. Riedel, The influence of pyrolysis temperature on the electrochemical behavior of porous carbon-rich SiCN polymer-derived ceramics, Solid State Ionics 315 (2018) 59–64, https://doi.org/10.1016/j.ssi.2017.11.032.
[9] L.M. Reinold, Y. Yamada, M. Graczyk-Zajac, H. Munakata, K. Kanamura, R. Riedel, The influence of the pyrolysis temperature on the electrochemical behavior of carbon-rich SiCN polymer-derived ceramics as anode materials in lithium-ion batteries, J. Power Sources 282 (2015) 409–415, https://doi.org/10.1016/j.jpowsour.2015.02.074.
[10] J. Dahn, A. Wilson, W. Xing, G. Zank, Electrodes for Lithium Ion Batteries Using Polysilazanes Ceramic with Lithium, 1997.
[11] L. David, R. Bhandavat, U. Barrera, G. Singh, Silicon oxycarbide glass-graphene composite paper electrode for long-cycle lithium-ion batteries, Nat. Commun. 7 (2016), 10998, https://doi.org/10.1038/ncomms10998.
[12] S. Bin Mujib, Z. Ren, S. Mukherjee, D.M. Soares, G. Singh, Design, characterization, and application of elemental 2D materials for electrochemical energy storage, sensing, and catalysis, Mater. Adv. 1 (2020) 2562–2591, https://doi.org/10.1039/D0MA00428F.
[13] A.A. Hamedani, C.W. Ow-Yang, S. Hayat Soytas, Silicon nanocrystals-embedded carbon nanofibers from hybrid polyacrylonitrile – TEOS precursor as high-performance lithium-ion battery anodes, J. Alloys Compd. 909 (2022), 164734, https://doi.org/10.1016/j.jallcom.2022.164734.

[14] H. Tetik, J. Orangi, G. Yang, K. Zhao, S. Bin Mujib, G. Singh, M. Beidaghi, D. Lin, 3D printed MXene aerogels with truly 3D macrostructure and highly engineered microstructure for enhanced electrical and electrochemical performance, Adv. Mater. 34 (2022), 2104980, https://doi.org/10.1002/adma.202104980.

[15] A. Tolosa, M. Widmaier, B. Krüner, J.M. Griffin, V. Presser, Continuous silicon oxycarbide fiber mats with tin nanoparticles as a high capacity anode for lithium-ion batteries, Sustain. Energy Fuels 2 (2018) 215–228, https://doi.org/10.1039/c7se00431a.

[16] E.S. Pampal, E. Stojanovska, B. Simon, A. Kilic, A review of nanofibrous structures in lithium ion batteries, J. Power Sources 300 (2015) 199–215, https://doi.org/10.1016/j.jpowsour.2015.09.059.

[17] M.S. Kolathodi, L. David, M.A. Abass, G. Singh, Polysiloxane-functionalized graphene oxide paper: pyrolysis and performance as a Li-ion battery and supercapacitor electrode, RSC Adv. 6 (2016) 74323–74331, https://doi.org/10.1039/C6RA15746G.

[18] M. Ma, H. Wang, X. Li, K. Peng, L. Xiong, X. Du, Free-standing SiOC/nitrogen-doped carbon fibers with highly capacitive Li storage, J. Eur. Ceram. Soc. 40 (2020) 5238–5246, https://doi.org/10.1016/j.ceramint.2020.11.031.

[19] S. Dey, S. Bin Mujib, G. Singh, Enhanced Li-ion rate capability and stable efficiency enabled by MoSe2 nanosheets in polymer-derived silicon oxycarbide fiber electrodes, Nanomaterials 12 (2022) 553, https://doi.org/10.3390/nano12030553.

[20] Q. Chen, D. Jia, B. Liang, Z. Yang, Y. Zhou, D. Li, R. Riedel, T. Zhang, C. Gao, Electrospinning of pure polymer-derived SiBCN nanofibers with high yield, Ceram. Int. 47 (2021) 10958–10964, https://doi.org/10.1016/j.ceramint.2020.12.215.

[21] Z. Sang, X. Yan, L. Wen, D. Su, Z. Zhao, Y. Liu, H. Ji, J. Liang, S.X. Dou, A graphene-modified flexible SiOC ceramic cloth for high-performance lithium storage, Energy Storage Mater. 25 (2019) 876–884, https://doi.org/10.1016/j.ensm.2019.11.014.

[22] S. Bin Mujib, R. Cuccato, S. Mukherjee, G. Franchin, P. Colombo, G. Singh, Electrospun SiOC ceramic fiber mats as freestanding electrodes for electrochemical energy storage applications, Ceram. Int. 46 (2020) 3565–3573, https://doi.org/10.1016/j.ceramint.2019.10.074.

[23] S. Sarkar, A. Chunder, W. Fei, L. An, L. Zhai, Superhydrophobic mats of polymer-derived ceramic fibers, J. Am. Ceram. Soc. 91 (2008) 2751–2755, https://doi.org/10.1111/j.1551-2916.2008.02500.x.

[24] D.G. Shin, D.H. Riu, H.E. Kim, Web-type silicon carbide fibers prepared by the electrospinning of polycarbosilanes, J. Ceram. Process. Res. 9 (2008) 209–214.

[25] X. Guo, F. Xiao, J. Li, H. Zhang, Q. Hu, G. Li, H. Sun, Y. Feng, X. Guo, J. Lu, J. Liu, G. Wang, H. Gong, Enhanced electromagnetic wave absorption performance of SiCN(Fe) fibers by in-situ generated Fe3Si and CNTs, Ceram. Int. 47 (2021) 19582–19594, https://doi.org/10.1016/j.ceramint.2021.03.296.

[26] X. Guo, F. Xiao, J. Li, H. Zhang, Q. Hu, G. Li, H. Sun, Fe-doped SiCN composite fibers for electromagnetic waves absorption, Ceram. Int. 47 (2021) 1184–1190, https://doi.org/10.1016/j.ceramint.2020.08.236.

[27] F. Xiao, H. Sun, J. Li, X. Guo, H. Zhang, J. Lu, Z. Pan, J. Xu, Electrospinning preparation and electromagnetic wave absorption properties of SiCN fibers, Ceram. Int. 46 (2020) 12773–12781, https://doi.org/10.1016/j.ceramint.2020.02.046.

[28] Y. Liu, W. Yang, X. He, H. Hou, Tailored synthesis of amorphous SiCNO mesoporous fibers through combining a facile electrospinning process and microwave-assisted pyrolysis, Ceram. Int. 45 (2019) 8640–8645, https://doi.org/10.1016/j.ceramint.2019.01.184.

[29] O. Flores, T. Schmalz, W. Krenkel, L. Heymann, G. Motz, Selective cross-linking of oligosilazanes to tailored meltable polysilazanes for the processing of ceramic SiCN fibres, J. Mater. Chem. A. 1 (2013) 15406–15415, https://doi.org/10.1039/c3ta13254d.

[30] H. Ramlow, C. Marangoni, G. Motz, R.A.F. Machado, Statistical optimization of polysilazane-derived ceramic: electrospinning with and without organic polymer as a spinning aid for manufacturing thinner fibers, Chem. Eng. J. Adv. 9 (2022), 100220, https://doi.org/10.1016/j.ceja.2021.100220.

[31] B. Rowden, N. Garcia-Araez, Estimating lithium-ion battery behavior from half-cell data, Energy Rep. 7 (2021) 97–103, https://doi.org/10.1016/j.egyr.2021.02.048.

[32] D. Mailley, A. Hébraud, G. Schlatter, A review on the impact of humidity during electrospinning: from the nanofiber structure engineering to the applications, Macromol. Mater. Eng. 306 (2021), 2100115, https://doi.org/10.1002/mame.202100115.

[33] V. Fasano, M. Moffa, A. Camposeo, L. Persano, D. Pisignano, Controlled atmosphere electrospinning of organic nanofibers with improved light emission and waveguiding properties, Macromolecules 48 (2015) 7803–7809, https://doi.org/10.1021/acs.macromol.5b01377.

[34] P. Dibandjo, M. Graczyk-Zajac, R. Riedel, V.S. Pradeep, G.D. Soraru, Lithium insertion into dense and porous carbon-rich polymer-derived SiOC ceramics, J. Eur. Ceram. Soc. 32 (2012) 2495–2503, https://doi.org/10.1016/j.jeurceramsoc.2012.03.010.

[35] R. Kolb, C. Fasel, V. Liebau-Kunzmann, R. Riedel, SiCN/C-ceramic composite as anode material for lithium ion batteries, J. Eur. Ceram. Soc. 26 (2006) 3903–3908, https://doi.org/10.1016/j.jeurceramsoc.2006.01.009.

[36] L. David, D. Asok, G. Singh, Synthesis and extreme rate capability of Si-Al-C-N functionalized carbon nanotube spray-on coatings as li-ion battery electrode, ACS Appl. Mater. Interfaces 6 (2014) 16056–16064, https://doi.org/10.1021/am5052729.

[37] C. Liu, Z.G. Neale, G. Cao, Understanding electrochemical potentials of cathode materials in rechargeable batteries, Mater. Today 19 (2016) 109–123, https://doi.org/10.1016/j.mattod.2015.10.009.

[38] S. Wang, X. Hu, Y. Dai, Preparation and electrochemical performance of polymer-derived SiBCN-graphene composite as anode material for lithium ion batteries, Ceram. Int. 43 (2017) 1210–1216, https://doi.org/10.1016/j.ceramint.2016.10.065.

[39] D. Ahn, R. Raj, Thermodynamic measurements pertaining to the hysteretic intercalation of lithium in polymer-derived silicon oxycarbide, J. Power Sources 195 (2010) 3900–3906, https://doi.org/10.1016/j.jpowsour.2009.12.116.

[40] D. Su, Y.L. Li, Y. Feng, J. Jin, Electrochemical properties of polymer-derived SiCN materials as the anode in lithium ion batteries, J. Am. Ceram. Soc. 92 (2009) 2962–2968, https://doi.org/10.1111/j.1551-2916.2009.03317.x.

[41] A. Vashisth, S. Khatri, S.H. Hahn, W. Zhang, A.C.T. Van Duin, M. Naraghi, Mechanical size effects of amorphous polymer-derived ceramics at the nanoscale: experiments and ReaxFF simulations, Nanoscale 11 (2019) 7447–7456, https://doi.org/10.1039/c9nr00958b.

[42] Q. Chen, D. Li, X. Liao, Z. Yang, D. Jia, Y. Zhou, R. Riedel, Polymer-derived lightweight SiBCN ceramic nanofibers with high microwave absorption performance, ACS Appl. Mater. Interfaces 13 (2021) 34889–34898, https://doi.org/10.1021/acsami.1c07912.

[43] Y. Feng, N. Feng, Y. Wei, Y. Bai, Preparation and improved electrochemical performance of SiCN-graphene composite derived from poly(silylcarbondiimide) as Li-ion battery anode, J. Mater. Chem. A. 2 (2014) 4168–4177, https://doi.org/10.1039/c3ta14441k.

[44] M. Graczyk-Zajac, L.M. Reinold, J. Kaspar, P.V.W. Sasikumar, G.D. Soraru, R. Riedel, New insights into understanding irreversible and reversible lithium storage within SiOC and SiCN ceramics, Nanomaterials 5 (2014) 233–245, https://doi.org/10.3390/nano5010233.

[45] D. Ahn, R. Raj, Cyclic stability and C-rate performance of amorphous silicon and carbon based anodes for electrochemical storage of lithium, J. Power Sources 196 (2011) 2179–2186, https://doi.org/10.1016/j.jpowsour.2010.09.086.

[46] Y. Li, Y. Hu, Y. Lu, S. Zhang, G. Xu, K. Fu, S. Li, C. Chen, L. Zhou, X. Xia, X. Zhang, One-dimensional SiOC/C composite nanofibers as binder-free anodes for lithium-ion batteries, J. Power Sources 254 (2014) 33–38, https://doi.org/10.1016/j.jpowsour.2013.12.044.

[47] S.H. Baek, L.M. Reinold, M. Graczyk-Zajac, R. Riedel, F. Hammerath, B. Büchner, H.J. Grafe, Lithium dynamics in carbon-rich polymer-derived SiCN ceramics probed by nuclear magnetic resonance, J. Power Sources 253 (2014) 342–348, https://doi.org/10.1016/j.jpowsour.2013.12.065.

[48] H. Sun, K. Zhao, Atomistic origins of high capacity and high structural stability of polymer-derived SiOC anode materials, ACS Appl. Mater. Interfaces 9 (2017) 35001–35009, https://doi.org/10.1021/acsami.7b10906.

[49] Y. Feng, S. Dou, Y. Wei, Y. Zhang, X. Song, X. Li, V.S. Battaglia, Preparation and capacity-fading investigation of polymer-derived silicon carbonitride anode for lithium-ion battery, ACS Omega 2 (2017) 8075–8085, https://doi.org/10.1021/acsomega.7b01462.

[50] M. Wilamowska, M. Graczyk-Zajac, R. Riedel, Composite materials based on polymer-derived SiCN ceramic and disordered hard carbons as anodes for lithium-ion batteries, J. Power Sources 244 (2013) 80–86, https://doi.org/10.1016/j.jpowsour.2013.03.137.

[51] J. Zhang, C. Xu, Z. Liu, W. Wang, X. Xin, L. Shen, X. Zhou, J. Zhou, Q. Huang, Enhanced rate capability of polymer-derived SiCN anode material for electrochemical storage of lithium with 3-D carbon nanotube network dispersed in nanoscale, J. Nanosci. Nanotechnol. 15 (2015) 3067–3075, https://doi.org/10.1166/jnn.2015.9690.

[52] P.U. Nzereogu, A.D. Omah, F.I. Ezema, E.I. Iwuoha, A.C. Nwanya, Anode materials for lithium-ion batteries: a review, Appl. Surf. Sci. Adv. 9 (2022), 100233, https://doi.org/10.1016/j.apsadv.2022.100233.

[53] Y. Feng, Y. Wei, Z. Jia, Y. Zhang, V. Battaglia, G. Liu, Polymer-derived and sodium hydroxide-treated silicon carbonitride material as anodes for high electrochemical performance Li-ion batteries, ChemistrySelect 1 (2016) 309–317, https://doi.org/10.1002/slct.201600046.

[54] M. Klett, J.A. Gilbert, S.E. Trask, B.J. Polzin, A.N. Jansen, D.W. Dees, D. P. Abraham, Electrode behavior RE-visited: monitoring potential windows, capacity loss, and impedance changes in Li1.03(Ni0.5Co0.2Mn0.3)0.97O2/silicon-graphite full cells, J. Electrochem. Soc. 163 (2016) A875–A887, https://doi.org/10.1149/2.0271606jes.

[55] I.E. Monje, N. Sanchez-Ramirez, S.H. Santagneli, P.H. Camargo, D. Bélanger, S. B. Schougaard, R.M. Torresi, In situ-formed nitrogen-doped carbon/silicon-based materials as negative electrodes for lithium-ion batteries, J. Electroanal. Chem. 901 (2021), 115732, https://doi.org/10.1016/j.jelechem.2021.115732.

[56] P. Lv, H. Zhao, C. Gao, Z. Du, J. Wang, X. Liu, SiO-C dual-phase glass for lithium ion battery anode with high capacity and stable cycling performance, J. Power Sources 274 (2015) 542–550, https://doi.org/10.1016/j.jpowsour.2014.10.077.

[57] L. David, S. Bernard, C. Gervais, P. Miele, G. Singh, Facile synthesis and high rate capability of silicon carbonitride/boron nitride composite with a sheet-like morphology, J. Phys. Chem. C 119 (2015) 2783–2791, https://doi.org/10.1021/jp508075x.

[58] Z. Wu, W. Lv, X. Cheng, J. Gao, Z. Qian, D. Tian, J. Li, W. He, C. Yang, A nanostructured Si/SiOC composite anode with volume-change-buffering microstructure for lithium-ion batteries, Chem. Eur J. 25 (2019) 2604–2609, https://doi.org/10.1002/chem.201805255.

[59] B.-S. Lee, S.-B. Son, K.-M. Park, G. Lee, K.H. Oh, S.-H. Lee, W.-R. Yu, Effect of pores in hollow carbon nanofibers on their negative electrode properties for a lithium rechargeable battery, ACS Appl. Mater. Interfaces 4 (2012) 6702–6710, https://doi.org/10.1021/am301873d.

[60] I. Zeferino González, H.-C. Chiu, R. Gauvin, G.P. Demopoulos, Y. Verde-Gómez, Silicon doped carbon nanotubes as high energy anode for lithium-ion batteries, Mater. Today Commun. 30 (2022), 103158, https://doi.org/10.1016/j.mtcomm.2022.103158.

[61] R. Bhandavat, G. Singh, Stable and efficient Li-ion battery anodes prepared from polymer-derived silicon oxycarbide-carbon nanotube shell/core composites, J. Phys. Chem. C 117 (2013) 11899–11905, https://doi.org/10.1021/jp310733b.
[62] P.E. Sanchez-Jimenez, R. Raj, Lithium insertion in polymer-derived silicon oxycarbide ceramics, J. Am. Ceram. Soc. 93 (2010) 1127–1135, https://doi.org/10.1111/j.1551-2916.2009.03539.x.
[63] H. Fukui, H. Ohsuka, T. Hino, K. Kanamura, A Si-O-C composite anode: high capability and proposed mechanism of lithium storage associated with microstructural characteristics, ACS Appl. Mater. Interfaces 2 (2010) 999–1008, https://doi.org/10.1021/am100030f.